Fragment-Based Drug Design of Novel Pyranopyridones as Cell Active and Orally Bioavailable Tankyrase Inhibitors
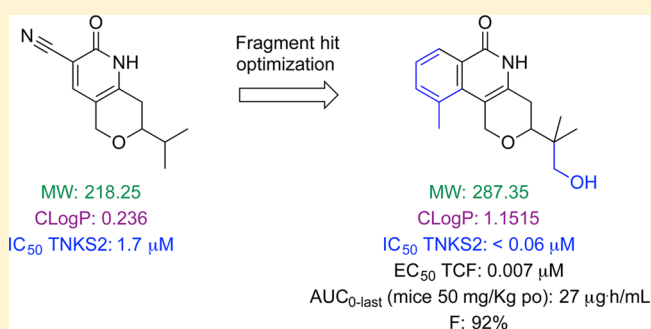
Javier de Vicente,*[†] Parcharee Tivitmahaisoon,[†] Pamela Berry,[‡] David R. Bolin,[†] Daisy Carvajal,[§] Wei He,[∥] Kuo-Sen Huang,[§] Cheryl Janson,[§] Lena Liang,[§] Christine Lukacs,[§] Ann Petersen,[†] Hong Qian,[§] Lin Yi,[†] Yong Zhuang,[∥] and Johannes C. Hermann[†]

[†]Discovery Chemistry, [‡]Non-clinical Safety, [§]Discovery Technologies, and [∥]Discovery Oncology, Small Molecule Research, Pharma Research & Early Development, Hoffmann-La Roche Inc., pRED, 340 Kingsland Street, Nutley, New Jersey 07110, United States

Ⓢ Supporting Information

ABSTRACT: Tankyrase activity has been linked to the regulation of intracellular axin levels, which have been shown to be crucial for the Wnt pathway. Deregulated Wnt signaling is important for the genesis of many diseases including cancer. We describe herein the discovery and development of a new series of tankyrase inhibitors. These pyranopyridones are highly active in various cell-based assays. A fragment/structure based optimization strategy led to a compound with good pharmacokinetic properties that is suitable for in vivo studies and further development.

MW: 218.25
CLogP: 0.236
IC$_{50}$ TNKS2: 1.7 μM

Fragment hit optimization

MW: 287.35
CLogP: 1.1515
IC$_{50}$ TNKS2: < 0.06 μM
EC$_{50}$ TCF: 0.007 μM
AUC$_{0\text{-last}}$ (mice 50 mg/Kg po): 27 μg·h/mL
F: 92%

KEYWORDS: Tankyrase inhibitor, fragment based drug design, structure based drug design, oncology, Wnt, axin

The Wnt signaling pathway is a major cellular pathway controlling multiple biological processes.[1] The final step in Wnt signaling is characterized by either proteolysis of the transcription factor β-catenin (Wnt signaling "on") or the prevention of its proteolysis resulting in β-catenin dependent gene transcription (Wnt signaling "off"). The Wnt dependent β-catenin destruction complex is assembled by adenomatous polyposis coli (APC), axin, and glycogen synthase kinase 3α/β (GSK3α/β). The formation of the destruction complex relies on the availability of all its constituents with axin as the rate limiting component.[2] Overexpression of axin has been shown to counteract effects of nonfunctional APC and to cause degradation of β-catenin.[3] Many cancers have artificially high Wnt signaling.[4−6] This is often caused by mutations; for example, colorectal cancers are characterized by mutations in the APC protein that prevent it from forming the β-catenin destruction complex.[7−9] Targeting Wnt is therefore of interest for the potential treatment of various diseases including cancer.[10−12]

Regulation of axin levels is important for any cell as it has direct consequences on Wnt signaling. Axin2 is directly regulated through Wnt signaling itself, as its transcription is dependent on β-catenin.[13] Tankyrase enzymes 1 and 2 (TNKS1 and TNKS2), also called Poly ADP Ribose Polymerase (PARP) 5a and 5b, respectively, are important regulators of intracellular axin levels as they catalyze poly-ADP-ribosylation of axin, which subsequently leads to ubiquitination and degradation.[14] Recently discovered small molecule inhibitors of TNKS not only showed the ability to protect axin from degradation and to raise intracellular axin levels, but they were

also efficacious in cancer cell lines and various animal models.[14−16] While reported studies on tankyrase inhibitors are limited to preclinical studies,[16−23] we set out to discover new drug-like TNKS inhibitors suitable for in vivo studies with the potential for further development into clinical compounds.

We began by a biochemical screen of our in house fragment library against TNKS1 and TNKS2. Among the many validated hits, two sparked our interest; particularly, a pyranopyridone 1 and a benzopyrimidone 2 that share some similarity with XAV939, one of the first published TNKS inhibitors (Table 1).[14]

Both compounds showed favorable ligand efficiencies of about 0.5 with the all aromatic benzopyrimidone 2 being 10-fold more potent. We obtained a cocrystal structure of 1 complexed with TNKS2 and were able to confidently model the binding mode of 2 based on the publicly available crystal structure of XAV939 bound to TNKS2 (PDB code 3KR8[24]).[25]
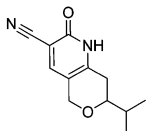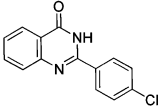
Inspection of the overlaid structures of 1 and 2 bound to TNKS2 (Figure 1) revealed commonalities and significant differences. The main recognition elements of the pyridone (1) or the pyrimidone (2) portions of the fragments to TNKS appeared almost identical, forming hydrogen bond interactions with Ser-1068, Tyr-1071, and Gly-1032. We hypothesized that the cyano group in the 3-position of the pyranopyridone ring of 1 was pointing into a hydrophobic spot of the pocket where it

Table 1. Structures and Biochemical Activity of Initial Fragment Hits

Compound	IC_{50} TNKS 2	TNKS2 Ligand Efficiency	IC_{50} TNKS 1
rac-1	1.7 μM	0.49	1 μM[a]
2	0.2 μM	0.51	0.14 μM[a]

[a]Throughout our optimization efforts we determined activities for TNKS1 and TNKS2. Since the activity of compounds against either enzyme changed similarly upon structural modifications, we will refer from here on only to the slightly less active TNKS2 activities. Full activity profiles for each compound are given in Table S1.
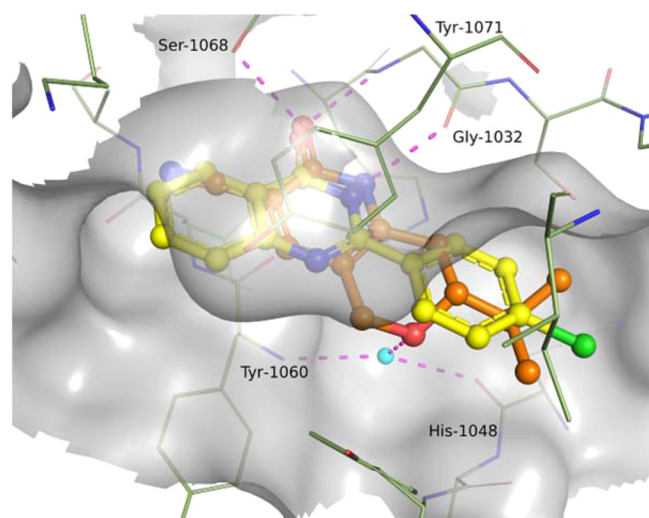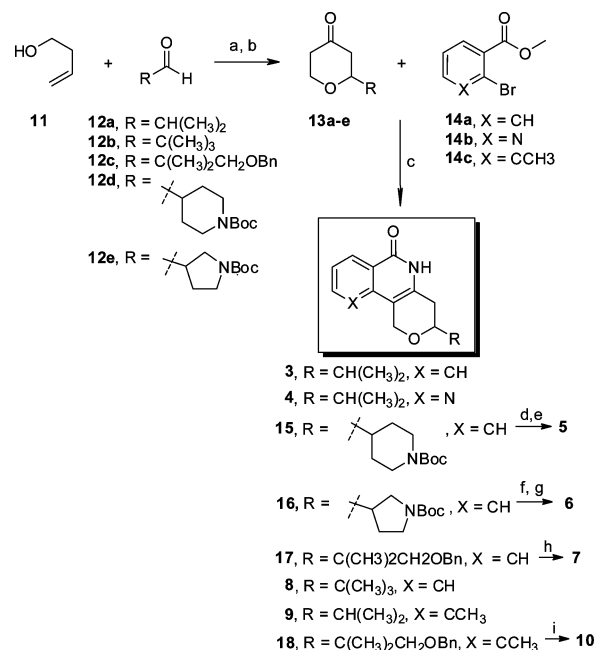

Figure 1. Crystal structure of **1** (carbon atoms in orange) bound to TNKS2 with **2** (carbon atoms in yellow) modeled in the active site and overlaid.[26] Oxygen atoms are in red (cyan for water molecules), nitrogen atoms in blue, and chlorine in green.

was not contributing to the binding affinity of the ligand. In contrast, the fused phenyl ring of the benzopyrimidone **2** maintains hydrophobic interactions. The aromatic ring is well packed with Tyr-1071 on one side in a skewed type face-to-face π-interaction and the Cβ-methylene group of Tyr-1060 on the opposite side. We were excited to see that the oxygen of the pyrane ring of **1** was accepting a hydrogen bond from a conserved water molecule that is tightly bound to Tyr-1060 and His-1048 (distance 3 Å). We decided to keep the pyrane ring in molecule **1** thereby maintaining the aliphatic sp^3 atoms in the scaffold and then replace the cyano group. The overlay suggested that merging the two fragments by incorporating the phenyl portion of the ~10× more potent benzopyrimidone core scaffold into the pyranopyridone in place of the nitrile group would be favorable. Subsequently compound **3** was

prepared (Scheme 1), which not only showed improved potency (Table 2), but remarkably also increased the already

Scheme 1. Synthetic Route to Pyranopyridones[a]

[a]Reagents, conditions, and yields (a) (i) TFA, CH₂Cl₂, rt; (ii) K₂CO₃, MeOH, rt, 63−94%; (b) PCC, SiO₂, CH₂Cl₂, rt, 73−83%; (c) (i) Pd₂dba₃, Xantphos, Cs₂CO₃, MW 90 °C; (ii) 7N NH₃ in MeOH, MW 140 °C 4−40%; (d) TFA, 140 °C, 77%; (e) EDCI, oxetane-3-carboxylic acid, DIPEA, DMF, rt, 46%; (f) acetyl chloride, MeOH, 0 °C to rt, 99% (g) methansulfonyl chloride, NMP, rt, 43%; (h) Pd(OH)₂ 20 wt %, HCl (cat), 1:1 dioxane/EtOH, 24%; (i) Pd(OH)₂ 20 wt %, HCl (cat), dioxane, 92%.
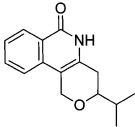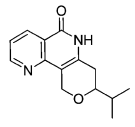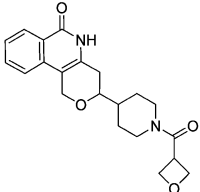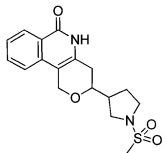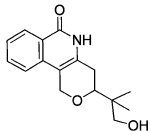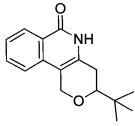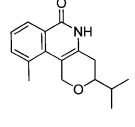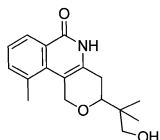
very desirable ligand efficiency of **2** to at least 0.56. Compound **3** was also reasonably potent in a functional luciferase cell based assay with an EC_{50} of 320 nM, suggesting favorable membrane permeability. However, the *in vivo* pharmacokinetic study (Table 2) in rats for this compound showed moderate to high clearance of 37 mL/min/kg consistent with the high intrinsic clearance predicted by rat liver microsomes.

The novel pyranopyridones were rapidly assembled in three steps (a−c, Scheme 1). A standard Prins cyclization of 3-buten-1-ol with commercially available aldehydes effectively yielded the 2-substituted pyrane building blocks. The alcohol at the 4-position was oxidized to a ketone with PCC. The final pyranopyridone scaffold was constructed by a palladium mediated regioselective ketone C-arylation to yield a tricyclic coumarine, which upon treatment with ammonia afforded the desired pyranopyridones.

Having established a concise synthesis of pyranopyridones, we set out to improve clearance, solubility, and cell potency with a focus on metabolic stability (Table 2). Aided by crystal structures, we aimed to increase solubility and possibly reduce clogP by introducing side chains and modifications consistent with our understanding of the binding site properties. In general, two areas seemed attractive for modifications of the initial pyranopyridone **3**; the fused phenyl ring and the isopropyl side chain on the other end of the molecule.

Although the fused phenyl ring portion is located in a narrow subpocket pointing toward a small exit channel of the binding

Table 2. Activity, Physicochemical, and DMPK Properties of Pyranopyrimidones

Compound[a]	IC_{50} Tankyrase 2 (nM)	EC_{50} TCF-luciferase cell assay (nM)	clogP	Solubility (μg/mL)[b]	Clint [category][c] Rat liver microsomes (μL/min/mg)	i.v. rat clearance (mL/min/kg)
3	< 60	320	1.7	5	114 [H]	37
4	93	810	1	13	50 [M]	10
5	< 60	31	0.44	13	28 [M]	nd
6	< 60	47	-0.5	28	27 [M]	47
7	< 60	341	0.65	66	6 [L]	nd
8	< 60	127	2.1	< 1	24 [M]	2
9	< 60	2	2.2	< 1	91 [H]	20
10	< 60	7	1.2	4	15 [M]	25

[a]Compounds 3−10 are racemic, and all the reported in vitro and in vivo data is with the racemic form. [b]LYSA kinetic solubility.[27] [c]Category of predicted clearance: low < 14 μL/min/mg; medium = 14−80 μL/min/mg; high > 80 μL/min/mg.

site, this subpocket displays minor patches where hydrophilic interactions seem possible, e.g., Glu-1138, Ser-1068, and Asn- 1064 (with bound water molecule). Modifications of the phenyl ring led to many compounds with improved properties;

however all of them showed loss of activity. One of the more promising compounds was the pyridine replacement **4**, which displayed slightly improved solubility (13 μg/mL), much better *in vivo* rat clearance (10 mL/min/kg), and only a 3-fold loss in cell potency.

The other area of modification, the isopropyl group, projects into an area where the binding site widens and allows larger side chains to fit. Many more interesting compounds were discovered by redesigning and replacing the isopropyl side chain, as exemplified by compounds **5**, **6**, and **7**. These types of compounds had similar or up to 10-fold higher cell potency, improved solubility, and often lower *in vitro* and *in vivo* clearance. The *t*-butyl compound **8** was discovered when trying to maximize the immediate hydrophobic contact next to the scaffold. Compound **8** was as predicted very potent but also surprisingly stable with a clearance of about 2 mL/min/kg. The low solubility of **8** led us to introduce hydrophilic solubilizing groups into the *t*-butyl. This area of the binding site seemed like it would tolerate hydrophilic groups of different sizes since it contains not only hydrophilic interaction surfaces but also many bulk and crystal water molecules to interact with. The most intriguing compound from this exercise was compound **7**.

Compound **7** retained all of the positive properties from compound **8** and had improved solubility of 66 μg/mL. The compound lacked high cell potency (341 nM), but that could have been potentially overcome by higher dosing and/or alternative routes of administration (e.g., *i.p.*). However, during the exploration of the fused phenyl ring of the scaffold we discovered a "magic methyl" (compound **9**), which did not improve properties, but boosted the potency by about 100-fold each time we introduced this motif into any of our more evolved compounds. Introduction of the methyl group into compound **7** led to compound **10**, which also showed vastly increased potency to 7 nM in cells (Figure 2).

The magic methyl fits nicely in a very small pocket, which is space limited on three sides by tyrosine residues Tyr-1050, Tyr-1060, and Tyr-1071 (Figure 2). In compounds lacking the methyl, this space is also bordered by the compound's phenyl
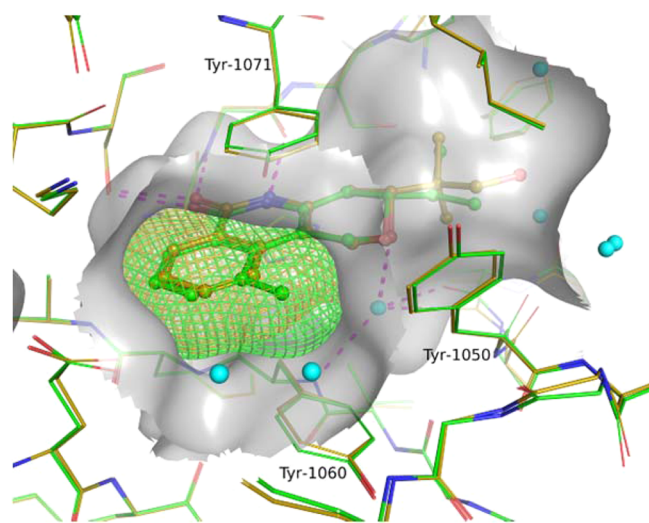
group moiety and remains empty or is filled by a water molecule that is offered only hydrophobic atoms for interaction. Filling this space with a small hydrophobic group like the methyl was thought to occupy this space perfectly, thereby potentially releasing an unfavorably bound water molecule. The improved potency of compounds bearing a methyl in that position may support this design hypothesis.

The methyl group in compound **10** provided the expected potency boost but caused a significant drop in solubility as compared to compound **7**. Hence the compound was further profiled in biorelevant FASSIF and FESSIF media solubility studies that revealed reasonable solubility at 50 and 143 μg/mL, respectively. The CACO2 permeability assay data for **10** (26 × 10^{-6}/sec) indicated that the compound was highly permeable.

Given the promising results thus far for compound **10**, it was decided to advance it into more in depth activity studies. We tested its ability to prevent axin degradation in an APC mutant cell line (DLD1). This study revealed that compound **10** was able to prevent the enhanced axin degradation in that cell line in a dose-dependent manner (graphical representation, Figure 3a). We then investigated whether or not compound **10** was able to inhibit mRNA production of β-catenin-dependent target genes such as Axin2 and TNFRSF19. Dose-dependent inhibition of expression was observed for both genes with compound **10** (Figure 3b).

Since these results showed that compound **10** was acting on target in a dose-dependent manner in cell based assays, we fully

Figure 2. Overlapping X-ray crystal structures of compounds **9** and **7** bound to TNKS2 showing the potency boosting methyl group. Compound **7** has carbon atoms colored in gold, **9** in green; oxygen atoms are in red (cyan for water molecules), and nitrogen atoms are colored blue.[26]
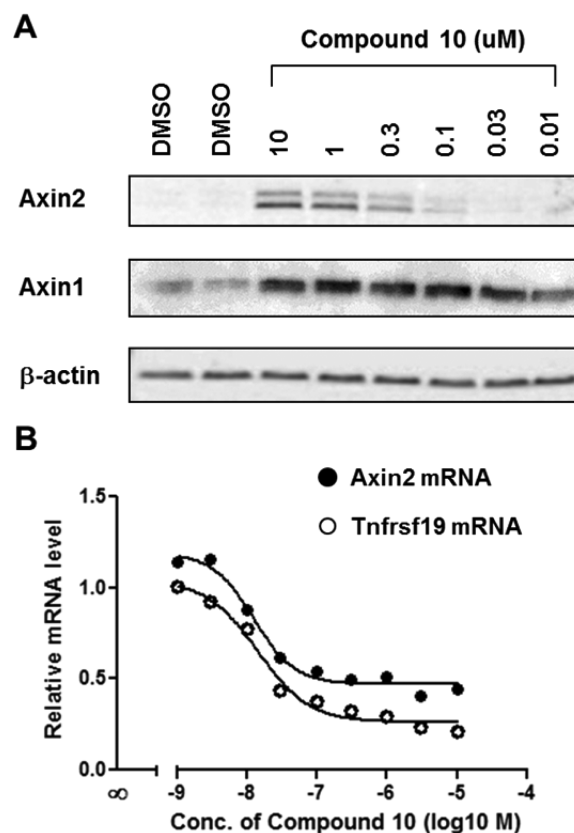

Figure 3. Axin protective effect of compound **10** in the APC mutant cell line DLD1. (A) Graphical gel representation of lack of axin1 and axin2 degradation. Controls are DMSO and tankyrase independent β-actin. (B) Dose-dependent inhibition of β-catenin target genes by compound **10**. Axin2 and TNFRSF19 expression is measured through qRT-PCR.

profiled **10** for its pharmacokinetic properties (Table 3) in order to assess its promise as an *in vivo* tool compound.

Table 3. Single Dose Pharmacokinetic Parameters of Compound 10 in Male C57BL/6J Mice

parameter	1 mg/kg iv	5 mg/kg po	50 mg/kg po
T_{max} (h)		0.25	0.25
C_{max} (μg/mL)		1.6	14
AUC$_{0\text{-last}}$ (μg·h/mL)	0.6	1.4	27
F (%)		49	92
Cl ((mL/min)/kg)	28		
Vdss (L/kg)	1.5		

Following administration to mice, compound **10** had moderate systemic clearance and volume of distribution and was absorbed rapidly and extensively. Oral bioavailability was reasonably high (49%) at the 5 mg/kg dose and increased to 92% at the 50 mg/kg dose. Overall the team was satisfied with the *in vitro* activity and pharmacokinetic profile of **10** and therefore confident that this compound can achieve sustainable high plasma levels for an *in vivo* proof of concept study.

In summary, our chemistry strategy followed a classical fragment/structure-based drug design approach supported by numerous in house crystal structures of key compounds and fragments. Merging two fragments with high ligand efficiency led to a novel lead series with favorable overall properties. This lead series was rapidly and effectively optimized toward favorable physicochemical properties and potency by increasing the already very high ligand efficiency. The resultant low molecular weight compounds are highly active in cells with single digit nanomolar potency. The optimized fragment-size lead compound **10** (MW = 287, cLogP = 1.2) was profiled in various Wnt signaling functional assays and displayed results consistent with on-target action. Single dose pharmacokinetic studies showed the compound to be a promising candidate for *in vivo* proof of concept studies.

ASSOCIATED CONTENT

Ⓢ Supporting Information
The Supporting Information is available free of charge on the ACS Publications website at DOI: 10.1021/acsmedchemlett.5b00251.

> Full synthetic details and characterization of synthetic intermediates and final products for all compounds described, enzymatic assay data for compounds **1−10**, crystallographic data details, and full description of pharmacokinetic studies and physicochemical assays (PDF)

Accession Codes
Structures are deposited in the RCSB Protein Data Bank under 5C5R, 5C5P, and 5C5Q (compounds **1**, **7**, and **9**, respectively).

AUTHOR INFORMATION

Corresponding Author
*Phone: 510-879-9321. E-mail: vicente_javier@hotmail.com.

Author Contributions
The manuscript was written through contributions of all authors. All authors have given approval to the final version of the manuscript.

Notes
The authors declare no competing financial interest.

ABBREVIATIONS
TNKS1, Tankyrase 1; TNKS2, Tankyrase 2; LYSA, lyophilization solubility assay; FASSIF, fasted-state simulated intestinal fluid; FESSIF, fed-state simulated intestinal fluid; APC, adenomatous polyposis coli; TCF, T-cell factor

REFERENCES
(1) Clevers, H. Wnt/β-Catenin Signaling in Development and Disease. *Cell* **2006**, *127* (3), 469−480.
(2) Lee, E.; Salic, A.; Krüger, R.; Heinrich, R.; Kirschner, M. W. The Roles of APC and Axin Derived from Experimental and Theoretical Analysis of the Wnt Pathway. *PLoS Biol.* **2003**, *1* (1), e10.
(3) Behrens, J.; Jerchow, B.-A.; Würtele, M.; Grimm, J.; Asbrand, C.; Wirtz, R.; Kühl, M.; Wedlich, D.; Birchmeier, W. Functional Interaction of an Axin Homolog, Conductin, with β-Catenin, APC, and GSK3β. *Science* **1998**, *280* (5363), 596−599.
(4) Klaus, A.; Birchmeier, W. Wnt signalling and its impact on development and cancer. *Nat. Rev. Cancer* **2008**, *8* (5), 387−398.
(5) Barker, N.; Clevers, H. Mining the Wnt pathway for cancer therapeutics. *Nat. Rev. Drug Discovery* **2006**, *5* (12), 997−1014.
(6) Reya, T.; Clevers, H. Wnt signalling in stem cells and cancer. *Nature* **2005**, *434* (7035), 843−850.
(7) Mori, Y.; Nagse, H.; Ando, H.; Horii, A.; Ichii, S.; Nakatsuru, S.; Aoki, T.; Miki, Y.; Mori, T.; Nakamura, Y. Somatic mutations of the APC gene in colorectal tumors: mutation cluster region in the APC gene. *Hum. Mol. Genet.* **1992**, *1* (4), 229−233.
(8) Powell, S. M.; Zilz, N.; Beazer-Barclay, Y.; Bryan, T. M.; Hamilton, S. R.; Thibodeau, S. N.; Vogelstein, B.; Kinzler, K. W. APC mutations occur early during colorectal tumorigenesis. *Nature* **1992**, *359* (6392), 235−237.
(9) Kinzler, K. W.; Vogelstein, B. Lessons from hereditary colorectal cancer. *Cell* **1996**, *87* (2), 159−170.
(10) Verkaar, F.; Zaman, G. J. R. New avenues to target Wnt/β-catenin signaling. *Drug Discovery Today* **2011**, *16* (1−2), 35−41. (b) MacDonald, B. T.; Tamai, K.; He, X. Wnt/beta-catenin signaling: components, mechanisms, and diseases. *Dev. Cell* **2009**, *17* (1), 9−26.
(11) MacDonald, B. T.; Tamai, K.; He, X. Wnt/beta-catenin signaling: components, mechanisms, and diseases. *Dev. Cell* **2009**, *17* (1), 9−26.
(12) Dihlmann, S.; von Knebel Doeberitz, M. Wnt/β-catenin-pathway as a molecular target for future anti-cancer therapeutics. *Int. J. Cancer* **2005**, *113* (4), 515−524.
(13) Leung, J. Y.; Kolligs, F. T.; Wu, R.; Zhai, Y.; Kuick, R.; Hanash, S.; Cho, K. R.; Fearon, E. R. Activation of AXIN2 Expression by β-Catenin-T Cell Factor. *J. Biol. Chem.* **2002**, *277* (24), 21657−21665.
(14) Huang, S.-M. A.; Mishina, Y. M.; Liu, S.; Cheung, A.; Stegmeier, F.; Michaud, G. A.; Charlat, O.; Wiellette, E.; Zhang, Y.; Wiessner, S.; Hild, M.; Shi, X.; Wilson, C. J.; Mickanin, C.; Myer, V.; Fazal, A.; Tomlinson, R.; Serluca, F.; Shao, W.; Cheng, H.; Shultz, M.; Rau, C.; Schirle, M.; Schlegl, J.; Ghidelli, S.; Fawell, S.; Lu, C.; Curtis, D.; Kirschner, M. W.; Lengauer, C.; Finan, P. M.; Tallarico, J. A.; Bouwmeester, T.; Porter, J. A.; Bauer, A.; Cong, F. Tankyrase inhibition stabilizes axin and antagonizes Wnt signalling. *Nature* **2009**, *461* (7264), 614−620.
(15) Chen, B.; Dodge, M. E.; Tang, W.; Lu, J.; Ma, Z.; Fan, C.-W.; Wei, S.; Hao, W.; Kilgore, J.; Williams, N. S.; Roth, M. G.; Amatruda, J. F.; Chen, C.; Lum, L. Small molecule-mediated disruption of Wnt-dependent signaling in tissue regeneration and cancer. *Nat. Chem. Biol.* **2009**, *5* (2), 100−107.
(16) Waaler, J.; Machon, O.; Tumova, L.; Dinh, H.; Korinek, V.; Wilson, S. R.; Paulsen, J. E.; Pedersen, N. M.; Eide, T. J.; Machonova, O.; Gradl, D.; Voronkov, A.; von Kries, J. P.; Krauss, S. A Novel

Tankyrase Inhibitor Decreases Canonical Wnt Signaling in Colon Carcinoma Cells and Reduces Tumor Growth in Conditional APC Mutant Mice. *Cancer Res.* **2012**, *72* (11), 2822−2832.

(17) Voronkov, A.; Holsworth, D. D.; Waaler, J.; Wilson, S. R.; Ekblad, B.; Perdreau-Dahl, H.; Dinh, H.; Drewes, G.; Hopf, C.; Morth, J. P.; Krauss, S. Structural Basis and SAR for G007-LK, a Lead Stage 1,2,4-Triazole Based Specific Tankyrase 1/2 Inhibitor. *J. Med. Chem.* **2013**, *56*, 3012−3023.

(18) Shultz, M. D.; Cheung, A. K.; Kirby, C. A.; Firestone, B.; Fan, J.; Chen, C. H.-T.; Chen, Z.; Chin, D. N.; DiPietro, L.; Fazal, A.; Feng, Y.; Fortin, P. D.; Gould, T.; Lagu, B.; Lei, H.; Lenoir, F.; Majumdar, D.; Ochala, E.; Palermo, M. G.; Pham, L.; Pu, M.; Smith, T.; Stams, T.; Tomlinson, R. C.; Toure, B. B.; Visser, M.; Wang, R. M.; Waters, N. J.; Shao, W. Identification of NVP-TNKS656: The Use of Structure-Efficiency Relationships To Generate a Highly Potent, Selective, and Orally Active Tankyrase Inhibitor. *J. Med. Chem.* **2013**, *56*, 6495−6511.

(19) Larsson, E. A.; Jansson, A.; Ng, F. M.; Then, S. W.; Panicker, R.; Liu, B.; Sangthongpitag, K.; Pendharkar, V.; Tai, S. J.; Hill, J.; Dan, C.; Ho, S. Y.; Cheong, W. W.; Poulsen, A.; Blanchard, S.; Lin, G. R.; Alam, J.; Keller, T. H.; Nordlund, P. Fragment-based ligand design of novel potent inhibitors of tankyrases. *J. Med. Chem.* **2013**, *56*, 4497−4508.

(20) Bregman, H.; Chakka, N.; Guzman-Perez, A.; Gunaydin, H.; Gu, Y.; Huang, X.; Berry, V.; Liu, J.; Teffera, Y.; Huang, L.; Egge, B.; Mullady, E. L.; Schneider, S.; Andrews, P. S.; Mishra, A.; Newcomb, J.; Serafino, R.; Strathdee, C. A.; Turci, S. M.; Wilson, C.; DiMauro, E. F. Discovery of Novel, Induced-Pocket Binding Oxazolidinones as Potent, Selective, and Orally Bioavailable Tankyrase Inhibitors. *J. Med. Chem.* **2013**, *56*, 4320−4342.

(21) Johannes, J. W.; Almeida, L.; Barlaam, B.; Boriack-Sjodin, P. A.; Casella, R.; Croft, R. O.; Dishington, A. P.; Gingipalli, L.; Gu, C.; Hawkins, J. L.; Holmes, J. L.; Howard, T.; Huang, J.; Ioannidis, S.; Kazmirski, S.; Lamb, M. L.; McGuire, T. M.; Moore, J. E.; Ogg, D.; Patel, A.; Pike, K. G.; Pontz, T.; Robb, G. R.; Su, N.; Wang, H.; Wu, X.; Zhang, H.-J.; Zhang, Y.; Zheng, X.; Wang, T. Pyrimidinone Nicotinamide Mimetics as Selective Tankyrase and Wnt Pathway Inhibitors Suitable for in Vivo Pharmacology. *ACS Med. Chem. Lett.* **2015**, *6*, 254−259.

(22) Nathubhai, A.; Wood, P. J.; Lloyd, M. D.; Thompson, A. S.; Threadgill, M. D. Design and Discovery of 2-Arylquinazolin-4-ones as Potent and Selective Inhibitors of Tankyrases. *ACS Med. Chem. Lett.* **2013**, *4*, 1173−1177.

(23) Voronkov, A.; Holsworth, D. D.; Waaler, J.; Wilson, S. R.; Ekblad, B.; Perdreau-Dahl, H.; Dinh, H.; Drewes, G.; Hopf, C.; Morth, J. P.; Krauss, S. Structural Basis and SAR for G007-LK, a Lead Stage 1,2,4-Triazole Based Specific Tankyrase 1/2 Inhibitor. *J. Med. Chem.* **2013**, *56*, 3012−3023.

(24) Karlberg, T.; Markova, N.; Johansson, I.; Hammarström, M.; Schütz, P.; Weigelt, J.; Schüler, H. Structural Basis for the Interaction between Tankyrase-2 and a Potent Wnt-Signaling Inhibitor. *J. Med. Chem.* **2010**, *53* (14), 5352−5355.

(25) Narwal, M.; Venkannagari, H.; Lehtio, L. Structural Basis of Selective Inhibition of Human Tankyrases. *J. Med. Chem.* **2012**, *55*, 1360−1367.

(26) *The PyMOL Molecular Graphics System*, version 1.5.0.4; Schrödinger, LLC: New York.

(27) Alsenz, J.; Kansy, M. High throughput solubility measurement in drug discovery and development. *Adv. Drug Delivery Rev.* **2007**, *59* (7), 546−567.